Solar Energy Materials & Solar Cells 107 (2012) 396–402

Contents lists available at SciVerse ScienceDirect

Solar Energy Materials & Solar Cells

journal homepage: www.elsevier.com/locate/solmat

Microanalysis of post-deposition annealing of $Cu(In,Ga)Se_2$ solar cells

Jörn Timo Wätjen *, Uwe Zimmermann, Marika Edoff **

Department of Engineering Sciences, Division of Solid State Electronics, Uppsala University, Box 534, SE-751 21 Uppsala, Sweden

ARTICLE INFO

Article history:
Received 14 September 2011
Received in revised form
25 June 2012
Accepted 20 July 2012
Available online 11 August 2012

Keywords:
CIGS
Three-stage process
Gradients
TEM
Post-deposition annealing
Microscopic *JV*-characterization

ABSTRACT

The influence of selenium background pressure during post-deposition annealing of $Cu(In,Ga)Se_2$ (CIGS) is investigated. Solar cells made from samples post-annealed with selenium showed the same solar cell parameters as references without any annealing treatment. Dark *JV* measurements of microscopic devices with sizes of 10 μm × 10 μm from the sample annealed with selenium showed good agreement with the corresponding macroscopic solar cells. Samples annealed without selenium showed degradation in terms of open circuit voltage and fill factor. Electron beam induced current (EBIC) imaging for these degraded solar cells revealed patches of reduced current. Microscopic *JV* measurements showed that the deterioration is not limited to these patches. Cross-sectional transmission electron microscopy analysis showed phase decomposition of the CIGS absorber in areas of the patches toward the back contact. We conclude that in addition to the local phase decomposition of the CIGS leading to patches in the EBIC image the anneal in vacuum without selenium background pressure also leads to other modifications of the CIGS layer influencing the interface region on a macroscopic scale.

1. Introduction

The compound semiconductor $Cu(In,Ga)Se_2$ often features gradients in the composition ratio $x=[Ga]/([Ga]+[In])$. Earlier simulations and experiments have concluded that Ga gradients can be engineered to reduce the recombination by a back surface field repelling electrons from the back contact thus lowering the saturation current density and resulting in increased open circuit voltage [1,2]. The formation of such a gradient strongly depends on the deposition method used and is attributed to Cu diffusion in combination with different mobilities for the diffusion of In and Ga ions, respectively [3–5]. These gradients are intrinsic to the often employed three-stage or multi-stage process so far delivering the highest solar cell efficiencies reaching up to 20.3% [6–8]. However, to our knowledge no studies have been conducted on the effect of post-deposition annealing on these gradients which may become important for deposition methods involving increased substrate temperatures and rapid thermal annealing processes [9,10].

Furthermore, local fluctuations in the solar cell material properties are reported to be a limitation in reaching high efficiency solar cells [11,12]. Some techniques measuring such fluctuations are cathodoluminescence, electron beam induced current and electron beam induced voltage [13]. However, these do not allow direct assessment of photovoltaic device parameters. An approach using photolithography to produce and characterize microscopic solar cells exists but does not offer the possibility of targeting specific regions of interest on fully processed solar cells [14].

Here, we present a method for *JV* characterization on the microscopic scale capable of targeting specific areas of interest on fully processed solar cells. We apply this method to study the influence of post-deposition annealing in vacuum with and without a selenium background pressure at high temperature on samples grown by a three-stage process in terms of device performance and composition from a microscopic as well as macroscopic perspective.

2. Methods

2.1. Device fabrication

The devices were deposited on substrates of 5 cm × 5 cm made from 1 mm thick sheets of soda lime glass (SLG). They were coated with a 300 nm DC sputtered Mo back contact layer according to our baseline procedure [15]. The $Cu(In,Ga)Se_2$ (CIGS) absorber layers were grown by a three-stage process using resistive co-evaporation of elemental Cu, In and Ga from fast acting open boat sources and a mass spectrometer to control the metal evaporation rates. A more detailed description is given in Schleussner et al. [18]. The selenium crucible source was kept at a constant temperature ensuring selenium excess during the deposition process. The substrate

---

* Corresponding author.
** Principal corresponding author.
E-mail addresses: timo.watjen@angstrom.uu.se (J. Timo Wätjen), uwe.zimmermann@angstrom.uu.se (U. Zimmermann), marika.edoff@angstrom.uu.se (M. Edoff).

0927-0248/$ - see front matter © 2012 Elsevier B.V. All rights reserved.
http://dx.doi.org/10.1016/j.solmat.2012.07.026

temperature during the processes was initially 450 °C and was increased to 530 °C at the beginning of the second stage and maintained at this level until the absorber layer deposition was complete. The temperatures were calibrated with a thermocouple implanted into a CIGS and Mo coated glass substrate.

After the absorber layer deposition a post-deposition treatment was applied. The post-deposition treatment consisted of keeping the substrate in vacuum at a constant temperature of 550 °C for 1 h after complete absorber layer deposition either with or without selenium, further referred to as 550wSe and 550woSe, before allowing for further cooling down. During the annealing the selenium source was either kept at the same temperature as during evaporation or was turned off. The chamber was purged with dry nitrogen when a substrate temperature between 100 °C and 110 °C was reached after which the samples were unloaded. Subsequently, the samples were further processed according to our baseline procedure and a 50 nm CdS buffer layer was applied using a chemical bath deposition process (CBD). The time span between sample unloading and CBD was kept at 12 min to ensure similar exposure to ambient atmosphere for all samples. A double layer of RF-sputtered intrinsic ZnO and Al-doped ZnO, 50 nm and 400 nm thick, respectively, serves as transparent front contact. Concluding the device fabrication, an e-beam evaporated Ni–Al–Ni current collecting grid was applied to the front contact and the cell area defined to 0.5 cm^2 using mechanical scribing.

For each post-deposition annealed sample a reference sample from the same day exists. They are distinguished from the corresponding annealing processes with the suffix "-Ref". The reference sample was deposited with the same deposition conditions as used for the post-deposition annealed sample except for omitting the annealing step. The reference samples were allowed to cool down immediately after the absorber layer deposition. This is necessary to monitor process stability and enable a day-to-day comparison between samples as small changes in elemental composition may occur over a period of several days.

2.2. Device characterization

For each sample a piece was removed prior to CBD deposition and used for elemental composition analysis of the absorber layer using X-ray fluorescence (XRF) performed on a Spectro X-lab 2000. A reference sample of known composition was used to calibrate the XRF measurements.

Solar cell parameters were obtained from current–voltage measurements (*JV*) at a device temperature of 25 °C under illumination by a calibrated ELH tungsten halogen lamp. The saturation current density and diode ideality factor were evaluated according to a method suggested by Hegedus and Shafarman [16].

Electron beam induced current (EBIC) and secondary electron (SE) images of finished solar cell stacks were acquired on a FEI Strata DB235 dual beam system operated with a primary electron energy of 15 keV. An AMETEK Model 181 low-noise current amplifier was used for EBIC imaging.

Microscopic devices with areas of 10 μm × 10 μm were prepared from fully processed solar cells using the 30 kV Ga$^+$ focused ion beam (FIB) of the dual beam system. The active device areas were defined by first applying a protective mask by electron and ion beam assisted deposition of Pt from a precursor gas as shown in Fig. 1(a) and (b). Concurrently, a thinner layer of residual Pt was formed in the proximity of the protective mask. Subsequently, the FIB was used to remove parts of the front contact ZnO layer around the mask until first perforations occurred as depicted in Fig. 1(c) and (d). The thin layer of remaining residual Pt was removed by exposing the sample briefly to the ion beam (d) resulting in an exposed ZnO layer, as shown in (e). The ZnO and CdS layers were subsequently removed by a short dip in dilute hydrochloric acid (0.04 M). As illustrated in Fig. 1(f) this results in an electrically isolated front contact. This is confirmed by cross-sectional imaging of a finished microscopic device in Fig. 2. The combination of focused ion beam and wet etching minimized both ion beam induced damage to the absorber layer as well as underetching of the mask, as indicated in the image, to a few hundred nanometers.

A Karl Suss PM8 probe station equipped with tungsten needles of 1 μm tip radius was used to contact the microscopic devices and electrical characterization was carried out with a HP 4115A semiconductor parameter analyzer. The method employed for evaluation of saturation current density and diode ideality factor

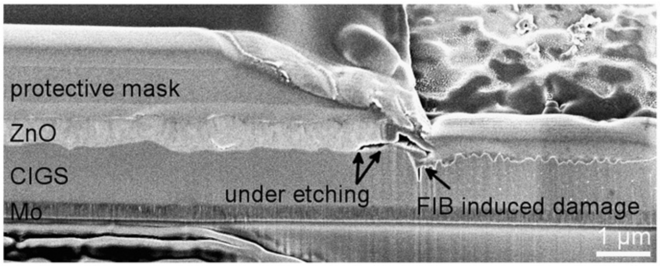

Fig. 2. Cross-sectional image of a microscopic device showing the Pt mask with intact solar cell layer stack beneath it. The front contact to the right side of the mask has been removed and under-etching of the mask is limited to a few hundred nanometers as indicated.

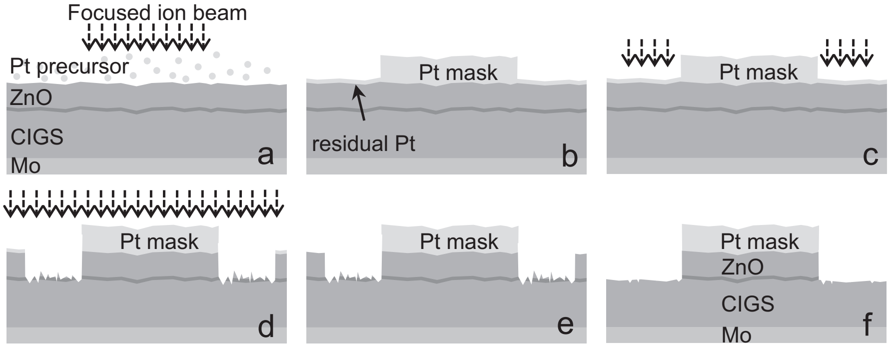

Fig. 1. Illustration of the process scheme used to obtain 10 μm × 10 μm devices from fully processed solar cells. A Pt containing precursor gas is decomposed under irradiation of a focused ion beam to locally deposit a Pt layer as shown in (a). Besides the formed Pt mask, shown in (b) a thin layer of residual Pt is formed outside of the targeted area. In (c) the FIB is utilized to cut through the residual Pt and front contact ZnO layers in the vicinity of the Pt mask. To remove the remaining residual Pt a larger sample area is briefly exposed to the ion beam in (d). As illustrated in (e) this leaves the ZnO surface exposed with a trench near the Pt mask only partially covered with ZnO. After wet-etching with dilute hydrochloric acid this results in an isolated front contact (f).